Transference of Fermi Contour Anisotropy to Composite Fermions

Insun Jo,[1] K. A. Villegas Rosales,[1] M. A. Mueed,[1] L. N. Pfeiffer,[1] K. W. West,[1] K. W. Baldwin,[1] R. Winkler,[2] Medini Padmanabhan,[3] and M. Shayegan[1]

[1]*Department of Electrical Engineering, Princeton University, Princeton, New Jersey 08544, USA*
[2]*Department of Physics, Northern Illinois University, DeKalb, Illinois 60115, USA*
[3]*Physical Sciences Department, Rhode Island College, Providence, Rhode Island 02908, USA*

(Received 20 January 2017; published 7 July 2017)

There has been a surge of recent interest in the role of anisotropy in interaction-induced phenomena in two-dimensional (2D) charged carrier systems. A fundamental question is how an anisotropy in the energy-band structure of the carriers at zero magnetic field affects the properties of the interacting particles at high fields, in particular of the composite fermions (CFs) and the fractional quantum Hall states (FQHSs). We demonstrate here tunable anisotropy for holes and hole-flux CFs confined to GaAs quantum wells, via applying *in situ* in-plane strain and measuring their Fermi wave vector anisotropy through commensurability oscillations. For strains on the order of 10^{-4} we observe significant deformations of the shapes of the Fermi contours for both holes and CFs. The measured Fermi contour anisotropy for CFs at high magnetic field (α_{CF}) is less than the anisotropy of their low-field hole (fermion) counterparts (α_F), and closely follows the relation $\alpha_{CF} = \sqrt{\alpha_F}$. The energy gap measured for the $\nu = 2/3$ FQHS, on the other hand, is nearly unaffected by the Fermi contour anisotropy up to $\alpha_F \sim 3.3$, the highest anisotropy achieved in our experiments.

DOI: 10.1103/PhysRevLett.119.016402

High-mobility, two-dimensional (2D) charged carriers at high perpendicular magnetic fields B and low temperatures exhibit rich many-body physics driven by Coulomb interaction. Examples include the fractional quantum Hall state (FQHS), Wigner crystal, and stripe phase [1,2]. Recently, the role of *anisotropy* has become a focus of new studies [3–23]. This interest has been amplified by the recognition that, although the FQHSs at fillings $1/q$ (q = odd integer) are well described by Laughlin's wave function with a rotational symmetry [24], there is a geometric degree of freedom associated with the anisotropy of the 2D carrier system [8].

The fundamental issue we address here is how the anisotropy of the energy-band structure of the low-field carriers transfers to the interacting particles at high B and, in particular, to the FQHSs and composite fermions (CFs). The latter are electron-flux quasiparticles that form a Fermi sea at a half-filled Landau level [2,25], and provide a simple explanation for the nearby FQHSs [26]. Because CFs are generated entirely by interactions and are thus not adiabatically connected with the zero-field particles, there is no agreement yet as to what properties of the zero-field particles, if any, the CFs inherit. While some theories predict that the CF Fermi contour anisotropy (α_{CF}) should be the same as the zero-field (fermion) contour anisotropy (α_F) [3,23], others conclude that α_{CF} is noticeably smaller than α_F [20–22]. This question was also addressed in several recent experimental studies. For 2D electrons occupying AlAs conduction-band valleys with an anisotropic effective mass, a pronounced *transport* anisotropy

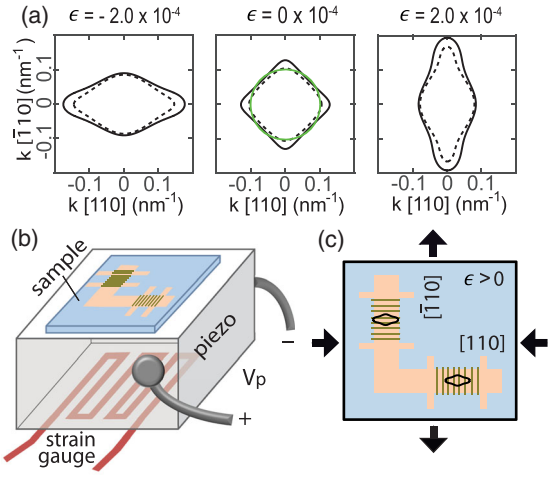

FIG. 1. (a) Calculated Fermi contours of GaAs holes at density $p = 1.8 \times 10^{11}$ cm^{-2} as a function of strain ϵ along the [1̄10] direction. Solid and dashed contours represent two spin-split subbands; the green circle with radius $k_0 = \sqrt{2\pi p}$ shows a spin-degenerate, circular Fermi contour at the same density. (b) Schematic of the experimental setup showing a thinned GaAs wafer glued on a piezo actuator. A strain gauge mounted underneath measures the strain along [1̄10]. (c) Sample fabricated to an L-shaped Hall bar has regions with electron-beam resist gratings on the surface. Thick arrows indicate the deformation of the crystal when a positive voltage V_P is applied to the piezo. The resulting deformed cyclotron orbits are shown in black; note that these are rotated by 90° with respect to the Fermi contours in reciprocal space. The shapes of the orbits and therefore the Fermi contours are determined via commensurability oscillations measurements.

was reported for CFs, but the anisotropy of the CF *Fermi contour* could not be measured because of the insufficient sample quality [5]. More recently, experiments probed the Fermi contour anisotropy of low-field carriers (both electrons and holes), and of CFs in GaAs quantum wells by subjecting them to an additional parallel magnetic field ($B_\parallel$) [12–16]. However, the $B_\parallel$-induced anisotropy is primarily caused by the coupling between the in-plane and out-of-plane motions of the carriers, rendering a theoretical understanding of the data challenging. Furthermore, a strong $B_\parallel$ can lead to a bilayerlike charge distribution [15].

As highlighted in Fig. 1, we demonstrate a simple yet powerful technique to tune and probe the anisotropy of both low-field carriers and high-field CFs *without* applying $B_\parallel$. The experiments consist of subjecting the sample, a GaAs 2D hole system (2DHS), to strain [27–30] and measuring α_F and α_{CF} via commensurability oscillations measurements. We find that, for a given value of strain, CFs are less anisotropic than their low-field 2D hole counterparts, and the anisotropies are related through a simple empirical relation: $\alpha_{CF} = \sqrt{\alpha_F}$. In contrast, the measured energy gap of the $\nu = 2/3$ FQHS remains almost constant even for α_F as large as 3.3. Our results allow a direct and quantitative comparison with theoretical predictions.

Figure 1(a) shows the results of numerical calculations for the strain-induced Fermi contour anisotropy of our sample, a 2DHS confined to a 175-Å-wide GaAs (001) quantum well [31–33]. The self-consistent calculations are based on an 8×8 Kane Hamiltonian [30,34,35]. Without strain ($\epsilon = 0$), the Fermi contour of holes is fourfold symmetric but is split into two contours because of the spin-orbit interaction [35]. The minority-spin contour is nearly circular while the majority-spin contour is warped. When tensile strain ($\epsilon > 0$) is applied along $[\bar{1}10]$, the hole Fermi contours become elongated along $[\bar{1}10]$ and shrink along the [110] direction [30,34–38]. On the other hand, compressible strain ($\epsilon < 0$) has the opposite effect [Fig. 1(a)]. Our experimental setup for applying *in situ* tunable strain to the sample is shown in Figs. 1(b) and 1(c) [28]. An L-shaped Hall bar is etched into the GaAs wafer which is thinned to ~120 μm and glued on one surface of a stacked piezo actuator. When a voltage $V_P > 0$ ($V_P < 0$) is applied to the piezo, the sample expands (contracts) along $[\bar{1}10]$. This is monitored using a strain gauge glued to the opposite face of the piezo [28–30].

In order to measure the Fermi wave vectors, we fabricate periodic gratings of negative electron-beam resist, with period $a = 200$ nm, on the surface of the L-shaped Hall bar [Fig. 1(c)]. The grating induces a periodic strain onto the GaAs surface, which in turn results in a small periodic modulation of the 2DHS density via the piezoelectric effect [32,33,39]. In the presence of B, when the cyclotron motion of holes becomes commensurate with a, the magnetoresistance shows oscillations whose minima positions are directly related to the carriers' Fermi wave vector in the direction perpendicular to the current [12,32,39,40]. Figure 1(c) shows an example when tensile strain is applied along $[\bar{1}10]$; the elongated cyclotron orbits under a finite B are indicated by black curves.

Figure 2(a) shows magnetoresistance traces for $\epsilon = -1.8 \times 10^{-4}$. The red and blue traces are from the patterned regions along the [110] and $[\bar{1}10]$ directions, respectively, while the

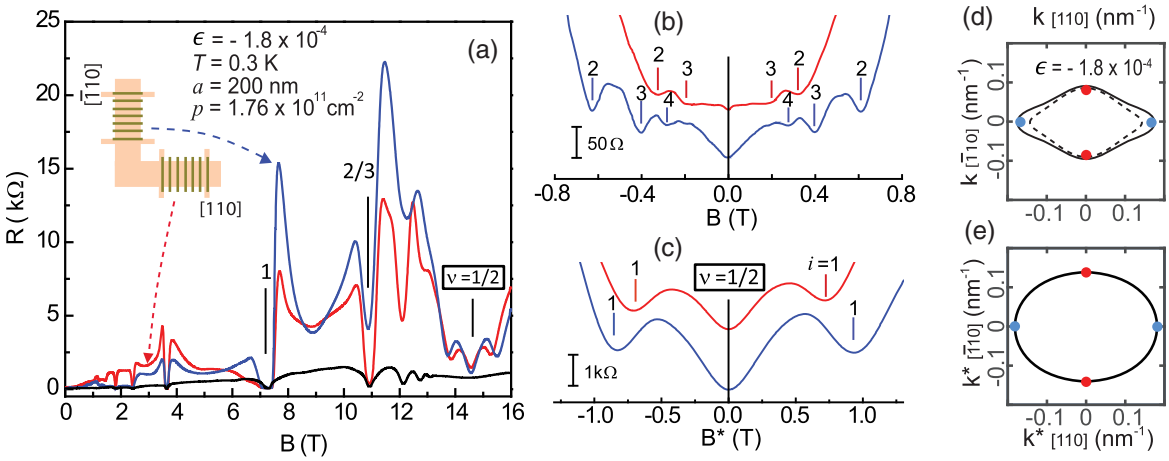

FIG. 2. (a) Magnetoresistance traces taken from different regions of the Hall bar when strain $\epsilon = -1.8 \times 10^{-4}$ is applied along $[\bar{1}10]$. The red and blue traces are for the patterned regions along the [110] and $[\bar{1}10]$ arms, while the black trace is for an unpatterned region. (b), (c) The red and blue traces in (a) are shown enlarged, exhibiting commensurability features for holes at low fields (b), and for CFs at high fields (c) near Landau level filling factor $\nu = 1/2$. The effective field for CFs in (c) is shown as B^*. The vertical lines in (b) and (c) indicate the positions of minima satisfying the commensurability conditions for holes and CFs (see text). (d) Calculated Fermi contours of spin-split holes at $p = 1.8 \times 10^{11}$ cm^{-2} and $\epsilon = -1.8 \times 10^{-4}$. Red and blue dots represent the measured Fermi wave vectors along the $[\bar{1}10]$ and [110] directions, using traces in (b). (e) An elliptical Fermi contour for CFs based on the measured Fermi wave vectors, using traces in (c).

black trace is for an unpatterned region. The red and blue traces exhibit commensurability features for holes near $B = 0$ [Fig. 2(b)] and for CFs near $\nu = 1/2$ [Fig. 2(c)]. To analyze the low-field hole data, we use the *electrostatic* commensurability condition [32,39,41–44] for the minima positions, $2R_c/a = i - 1/4$ $(i = 1, 2, 3, \ldots)$ where $2R_c = 2\hbar k/eB$ is the cyclotron orbit diameter, k is the 2DHS Fermi wave vector perpendicular to the current, and a is the period of the density modulation. For CFs, we observe commensurability features near $\nu = 1/2$, or $B_{1/2} = 14.5$ T [Fig. 2(c)]. The positions of minima around $\nu = 1/2$ yield the Fermi wave vector of CFs (k^*) according to the *magnetic* commensurability condition [33,45,46], $2R_c^*/a = i + 1/4$, where the CF cyclotron diameter $2R_c^* = 2\hbar k^*/eB^*$ and $B^* = B - B_{1/2}$ is the effective field for CFs [47,48].

In Fig. 2(d) we mark the measured Fermi wave vectors for holes with red and blue dots along $[\bar{1}10]$ and $[110]$. Although theoretical calculations for holes predict two spin subbands with different Fermi wave vectors [black solid and dashed curves in Fig. 2(d)], we measure a single k for each direction from the commensurability features [32,49]. The measured $k_{[\bar{1}10]}$ (red dots) and $k_{[110]}$ (blue dots) are close to the average calculated Fermi wave vectors for the two spin subbands. Figure 2(e) shows k^* measured for CFs with red and blues dots. We depict the Fermi contour as an ellipse because there are no theoretical calculations available for CFs, and also the area of an ellipse spanned by the two measured k^* accounts for the density of CFs which are fully spin polarized at high fields [33]. Note that the CF Fermi contour anisotropy $\alpha_{CF} \equiv k^*_{[\bar{1}10]}/k^*_{[110]} = 0.77$, which is closer to unity than the 2D hole anisotropy $\alpha_F \equiv k_{[\bar{1}10]}/k_{[110]} = 0.53$. Quantitatively, we find $\alpha_{CF} = \sqrt{\alpha_F}$ to within 5%; see below.

Next we demonstrate the tunability of CF Fermi contour anisotropy via strain. Figures 3(a) and 3(b) show magnetoresistance traces near $\nu = 1/2$, taken along $[\bar{1}10]$ and $[110]$, at different strains. In each panel, the green trace represents the $\epsilon = 0$ case, where the Fermi contour is essentially isotropic and $k^* = k_0^* = \sqrt{4\pi p}$ [30]. The traces shown above the green trace are for tensile strain ($\epsilon > 0$) while those below are for compressive strain ($\epsilon < 0$). In Fig. 3(a) the positions of resistance minima move towards (away from) $B^* = 0$ for $\epsilon > 0$ ($\epsilon < 0$), while the opposite is true for Fig. 3(b). These observations imply a distortion in the shape of CF cyclotron orbits as depicted in the side panels of Figs. 3(a) and 3(b).

Figure 3(c) summarizes the measured k^* along $[\bar{1}10]$ and $[110]$, normalized by k_0^*. Comparing k^* values for compressive and tensile cases, the change of k^* for $\epsilon > 0$ is larger than for $\epsilon < 0$. This asymmetry reflects the response of the 2DHS Fermi contour to the applied strain; note that in Fig. 1(a) $\epsilon > 0$ deforms the hole Fermi contour more significantly than the $\epsilon > 0$ does. We also find that the geometric means of k^*/k_0^* along the two perpendicular directions remain close to unity [Fig. 3(d)]. This suggests that CF Fermi contours are nearly elliptical, although we cannot exclude a more complex shape.

Figure 4 illustrates the highlight of our study: comparison of strain-induced Fermi contour anisotropy for CFs and

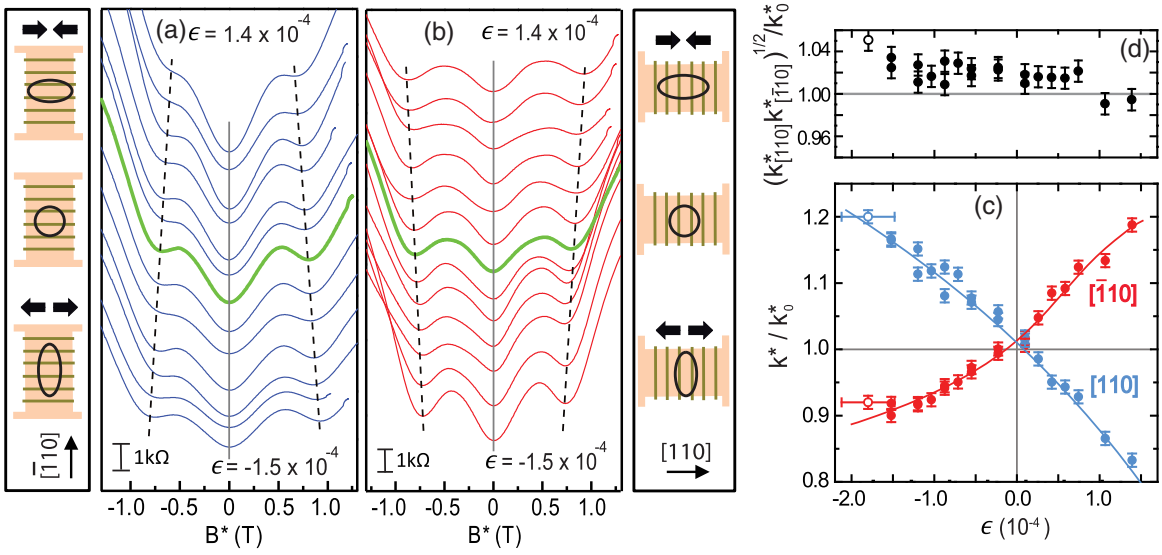

FIG. 3. (a) and (b) Commensurability features for CFs near $\nu = 1/2$ along the $[\bar{1}10]$ and $[110]$ directions of the Hall bar as strain ϵ is varied between -1.5 and $+1.4 \times 10^{-4}$. Green traces are for the $\epsilon = 0$ case. Dashed lines are guides to the eye to follow the evolution of the CF commensurability minima. Left panel of (a) and right panel of (b) show the direction of the strain (thick arrows), and shapes of CF cyclotron orbits (circle and ellipses). (c) Measured CF Fermi wave vector k^* along the $[\bar{1}10]$ (red) and $[110]$ (blue) directions, normalized to k_0^*, are shown as a function of ϵ. The lines are guides to the eye. Open circles are from a different sample cooldown and represent the data shown in Fig. 2. (d) Geometric means of $k^*_{[110]}$ and $k^*_{[\bar{1}10]}$, normalized to k_0^*.

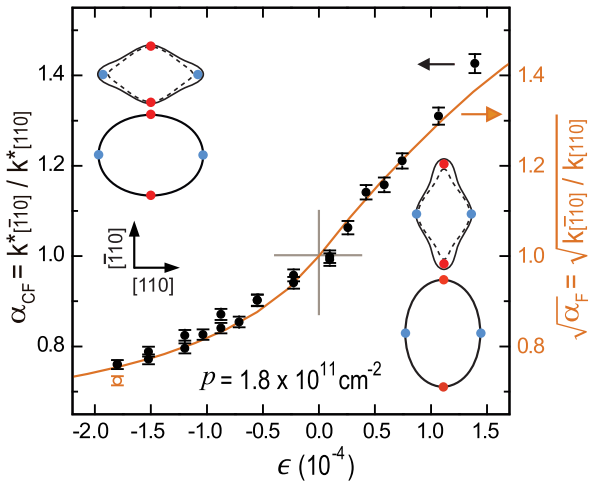

FIG. 4. Strain-dependent Fermi contour anisotropy of holes (α_F) and CFs (α_{CF}). Black circles are the measured α_{CF}. The orange curve represents the square root of the calculated α_F. The open orange circle shows the measured α_F for holes as described in Fig. 2. The left and right insets show the hole and CF Fermi contour shapes for $\epsilon = -1.5$ and 1.4×10^{-4}.

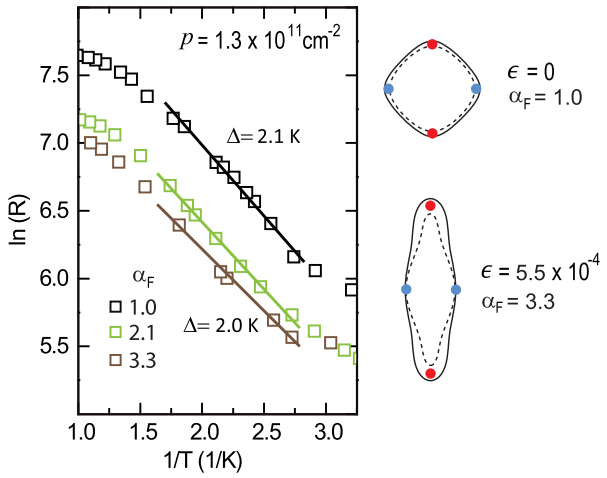

FIG. 5. Longitudinal resistance at $\nu = 2/3$ is recorded for an unpatterned region of the sample at different temperatures for energy gap (Δ) measurements, in cases of $\alpha_F = 1.0$, 2.1, and 3.3. The y-axis scale is $\ln(R)$, where R is measured in Ohms. The slopes of the straight lines yield the energy gaps. The calculated 2DHS Fermi contour shapes are shown on the right, where the red dots indicate the measured $k_{[\bar{1}10]}$ and blue dots are determined based on calculations for $p = 1.3 \times 10^{11}$ cm^{-2}.

holes. The measured anisotropy for CFs, $\alpha_{CF} = k^*_{[\bar{1}10]}/k^*_{[110]}$, is shown by black circles, and the *square root* of the calculated anisotropy for holes, $\alpha_F = k_{[\bar{1}10]}/k_{[110]}$, by an orange curve. Here we use, for each $k_{[\bar{1}10]}$ and $k_{[110]}$, the averaged values of k for the spin subbands, since experiments measure only a single k for each direction [49]. Remarkably, the measured α_{CF} for CFs essentially coincides with $\sqrt{\alpha_F}$ over the entire range of strains applied in the experiments. This is particularly striking because there are no fitting or adjustable parameters.

Lastly, we study the impact of anisotropy on the strength of FQHSs, focusing on the energy gap for the $\nu = 2/3$ state. The sample used for the measurements has $p = 1.3 \times 10^{11}$ cm^{-2}, and exhibits commensurability features only for holes along $k_{[\bar{1}10]}$. Moreover, using a different cooldown procedure [30], we achieved larger strain values (ϵ up to 5.5×10^{-4}), and anisotropy (α_F as large as 3.3) as shown in Fig. 5. The measured energy gap Δ, determined from the expression $R(T) \sim e^{-\Delta/2T}$, is 2.1 K for $\epsilon = 0$, and it decreases only to 2.0 K even for a large anisotropy $\alpha_F = 3.3$ [50]. The small decrease of Δ is consistent with recent theoretical predictions [23], suggesting that the FQHSs in the lowest Landau level are quite robust against anisotropy.

Returning to the Fermi contour anisotropy, our measurements (Fig. 4) provide quantitative evidence for a simple relation between the anisotropy of low-field fermions and high-field CFs: $\alpha_{CF} = \sqrt{\alpha_F}$. This appears to contradict some of the theories which predict that α_F and α_{CF} should be the same [3,23]. One can, however, qualitatively justify the square-root relation [5]. In an ideal, isotropic 2D system, the Coulomb interaction V_C ($\propto 1/\sqrt{x^2 + y^2}$) determines the physical parameters of CFs, including their effective mass m^*, which is linearly proportional to V_C [2,25]. At a given filling factor, V_C is quantified solely by the magnetic length $l_B = \sqrt{\hbar/eB}$ [2,25]. Now, a system with an anisotropic dispersion $\alpha_F \neq 1$ at $B = 0$ can be mapped to a system with an isotropic Fermi contour and an anisotropic V_C ($\propto 1/\sqrt{x^2\alpha_F + y^2/\alpha_F}$) using the coordinate transformations $x \to x/\sqrt{\alpha_F}$ and $y \to y\sqrt{\alpha_F}$. In such a system the strength of V_C at high fields thus depends not only on l_B but also on the direction; i.e., V_C anisotropy is α_F. If one assumes that CFs have a parabolic dispersion and an anisotropic m^* whose anisotropy follows linearly the anisotropy of V_C, then the *mass* anisotropy of CFs is given by α_F, implying that their Fermi wave vector anisotropy is proportional to $\sqrt{\alpha_F}$.

In conclusion, our results provide direct and quantitative evidence for the inheritance of Fermi contour anisotropy by CFs from their low-field fermion counterparts through a simple relation: $\alpha_{CF} = \sqrt{\alpha_F}$. While the discussion in the preceding paragraph serves as a plausibility argument for this relation, there is also some very recent rigorous theoretical justification. In their numerical calculations for anisotropic fermions with a parabolic band, Ippoliti *et al.* [51] find that the relation $\alpha_{CF} = \sqrt{\alpha_F}$ is indeed empirically obeyed [52]. It remains to be seen, both experimentally and theoretically, if the relation holds when the fermions' band deviates significantly from parabolic [14,53].

We acknowledge support by the DOE BES (No. DE-FG02-00-ER45841) Grant for measurements, and the NSF (Grants No. DMR 1305691, No. DMR 1310199, No. MRSEC DMR 1420541, and No. ECCS 1508925), the

Gordon and Betty Moore Foundation (Grant No. GBMF4420), and Keck Foundation for sample fabrication and characterization. We thank R. N. Bhatt, S. D. Geraedts, M. Ippoliti, J. K. Jain, and D. Kamburov for illuminating discussions.

[1] M. Shayegan, Flantland Electrons in High Magnetic Fields, in *High Magnetic Fields: Science and Technology*, edited by F. Herlach and N. Miura (World Scientific, Singapore, 2006), Vol. 3, p. 31.
[2] J. K. Jain, *Composite Fermions* (Cambridge University Press, Cambridge, England, 2007).
[3] D. B. Balagurov and Y. E. Lozovik, Phys. Rev. B **62**, 1481 (2000).
[4] M. Shayegan, E. P. De Poortere, O. Gunawan, Y. P. Shkolnikov, E. Tutuc, and K. Vakili, Phys. Status Solidi B **243**, 3629 (2006).
[5] T. Gokmen, M. Padmanabhan, and M. Shayegan, Nat. Phys. **6**, 621 (2010).
[6] E. Fradkin, S. A. Kivelson, M. J. Lawler, J. P. Eisenstein, and A. P. Mackenzie, Annu. Rev. Condens. Matter Phys. **1**, 153 (2010).
[7] M. Mulligan, C. Nayak, and S. Kachru, Phys. Rev. B **82**, 085102 (2010).
[8] F. D. M. Haldane, Phys. Rev. Lett. **107**, 116801 (2011).
[9] J. Xia, J. P. Eisenstein, L. N. Pfeiffer, and K. W. West, Nat. Phys. **7**, 845 (2011).
[10] S. P. Koduvayur, Y. Lyanda-Geller, S. Khlebnikov, G. Csathy, M. J. Manfra, L. N. Pfeiffer, K. W. West, and L. P. Rokhinson, Phys. Rev. Lett. **106**, 016804 (2011).
[11] Y. Liu, S. Hasdemir, M. Shayegan, L. N. Pfeiffer, K. W. West, and K. W. Baldwin, Phys. Rev. B **88**, 035307 (2013).
[12] D. Kamburov, Y. Liu, M. Shayegan, L. N. Pfeiffer, K. W. West, and K. W. Baldwin, Phys. Rev. Lett. **110**, 206801 (2013).
[13] D. Kamburov, M. A. Mueed, M. Shayegan, L. N. Pfeiffer, K. W. West, K. W. Baldwin, J. J. D. Lee, and R. Winkler, Phys. Rev. B **89**, 085304 (2014).
[14] M. A. Mueed, D. Kamburov, Y. Liu, M. Shayegan, L. N. Pfeiffer, K. W. West, K. W. Baldwin, and R. Winkler, Phys. Rev. Lett. **114**, 176805 (2015).
[15] M. A. Mueed, D. Kamburov, M. Shayegan, L. N. Pfeiffer, K. W. West, K. W. Baldwin, and R. Winkler, Phys. Rev. Lett. **114**, 236404 (2015).
[16] M. A. Mueed, D. Kamburov, S. Hasdemir, L. N. Pfeiffer, K. W. West, K. W. Baldwin, and M. Shayegan, Phys. Rev. B **93**, 195436 (2016).
[17] N. Samkharadze, K. A. Schreiber, G. C. Gardner, M. J. Manfra, E. Fradkin, and G. A. Csáthy, Nat. Phys. **12**, 191 (2016).
[18] H. Wang, R. Narayanan, X. Wan, and F. Zhang, Phys. Rev. B **86**, 035122 (2012).
[19] R.-Z. Qiu, F. D. M. Haldane, X. Wan, K. Yang, and S. Yi, Phys. Rev. B **85**, 115308 (2012).
[20] B. Yang, Z. Papic, E. H. Rezayi, R. N. Bhatt, and F. D. M. Haldane, Phys. Rev. B **85**, 165318 (2012).
[21] K. Yang, Phys. Rev. B **88**, 241105 (2013).
[22] S. Johri, Z. Papic, P. Schmitteckert, R. N. Bhatt, and F. D. M. Haldane, New J. Phys. **18**, 025011 (2016).
[23] A. C. Balram and J. K. Jain, Phys. Rev. B **93**, 075121 (2016).
[24] R. B. Laughlin, Phys. Rev. Lett. **50**, 1395 (1983).
[25] B. I. Halperin, P. A. Lee, and N. Read, Phys. Rev. B **47**, 7312 (1993).
[26] J. K. Jain, Phys. Rev. Lett. **63**, 199 (1989).
[27] Throughout this Letter, we denote strain by $\epsilon = \epsilon_{[\bar{1}10]} - \epsilon_{[110]}$, where $\epsilon_{[\bar{1}10]}$ and $\epsilon_{[110]}$ are strains along the $[\bar{1}10]$ and $[110]$ directions and $\epsilon_{[110]} = -0.38\epsilon_{[\bar{1}10]}$; see Refs. [28,29].
[28] M. Shayegan, K. Karrai, Y. P. Shkolnikov, K. Vakili, E. P. De Poortere, and S. Manus, Appl. Phys. Lett. **83**, 5235 (2003).
[29] Y. P. Shkolnikov, K. Vakili, E. P. De Poortere, and M. Shayegan, Appl. Phys. Lett. **85**, 3766 (2004).
[30] See Supplemental Material at http://link.aps.org/supplemental/10.1103/PhysRevLett.119.016402 for a more detailed description of the strain effect.
[31] For details of our sample structure, see Refs. [32,33].
[32] D. Kamburov, H. Shapourian, M. Shayegan, L. N. Pfeiffer, K. W. West, K. W. Baldwin, and R. Winkler, Phys. Rev. B **85**, 121305 (2012).
[33] D. Kamburov, M. Shayegan, L. N. Pfeiffer, K. W. West, and K. W. Baldwin, Phys. Rev. Lett. **109**, 236401 (2012).
[34] G. L. Bir and G. E. Pikus, *Symmetry and Strain-Induced Effects in Semiconductors* (Wiley, New York, 1974).
[35] R. Winkler, *Spin-orbit Coupling Effects in Two-Dimensional Electron and Hole Systems* (Springer, Berlin, 2003).
[36] K. I. Kolokolov, A. M. Savin, S. D. Beneslavski, N. Ya. Minina, and O. P. Hansen, Phys. Rev. B **59**, 7537 (1999).
[37] B. Habib, J. Shabani, E. P. De Poortere, M. Shayegan, and R. Winkler, Phys. Rev. B **75**, 153304 (2007).
[38] J. Shabani, M. Shayegan, and R. Winkler, Phys. Rev. Lett. **100**, 096803 (2008).
[39] A. Endo, S. Katsumoto, and Y. Iye, Phys. Rev. B **62**, 16761 (2000).
[40] O. Gunawan, Y. P. Shkolnikov, E. P. De Poortere, E. Tutuc, and M. Shayegan, Phys. Rev. Lett. **93**, 246603 (2004).
[41] D. Weiss, K. von Klitzing, K. Ploog, and G. Weimann, Europhys. Lett. **8**, 179 (1989).
[42] R. W. Winkler, J. P. Kotthaus, and K. Ploog, Phys. Rev. Lett. **62**, 1177 (1989).
[43] R. R. Gerhardts, D. Weiss, and K. von Klitzing, Phys. Rev. Lett. **62**, 1173 (1989).
[44] C. W. J. Beenakker, Phys. Rev. Lett. **62**, 2020 (1989).
[45] J. H. Smet, S. Jobst, K. von Klitzing, D. Weiss, W. Wegscheider, and V. Umansky, Phys. Rev. Lett. **83**, 2620 (1999).
[46] S. D. M. Zwerschke and R. R. Gerhardts, Phys. Rev. Lett. **83**, 2616 (1999).
[47] D. Kamburov, Y. Liu, M. A. Mueed, M. Shayegan, L. N. Pfeiffer, K. W. West, and K. W. Baldwin, Phys. Rev. Lett. **113**, 196801 (2014).
[48] In view of Ref. [47], we take the CF density to equal the minority carrier density in the lowest Landau level, and use the minimum position for $B^* > 0$ to extract the k^* of CFs.
[49] I. Jo, M. A. Mueed, L. N. Pfeiffer, K. W. West, K. W. Baldwin, R. Winkler, M. Padmanabhan, and M. Shayegan, Appl. Phys. Lett. **110**, 252103 (2017).

[50] The thermally activated regime of the data in Fig. 5 is limited, rendering the absolute values of the deduced gaps not very accurate. It is clear, however, that the three data sets for different α_F are essentially parallel to each other, implying that the energy gaps are very similar.

[51] M. Ippoliti, S. D. Geraedts, and R. N. Bhatt, Phys. Rev. B **95**, 201104 (2017).

[52] A similar relation can also be derived from Eq. (15) in Ref. [21], provided that the range of interaction (s) in the postulated Gaussian potential equals l_B.

[53] Quantifying the 2DHS Fermi contour "warping" by the geometric mean of $k_{[110]}/k_0$ and $k_{[\bar{1}10]}/k_0$, we note that this mean varies between 1.12 and 1.16 in the ϵ range of Fig. 4. (For a circular or an elliptical Fermi contour, the mean is unity). The equivalently defined parameter for CFs is closer to unity [see Fig. 3(d)], implying that CFs' Fermi contour is less warped than their zero-field counterparts. A similar conclusion was reached in Ref. [14].